Preprints of the 21st IFAC World Congress (Virtual)
Berlin, Germany, July 12-17, 2020

Stabilising the Light Spectrum of LED Solar Simulators Using LQG Control

J. Hofbauer * **M. Rudolph** * **S. Streif** **

* *Leipzig University of Applied Sciences (HTWK Leipzig); Laboratory for Industrial Measurement, 04277 Leipzig, Germany (e-mail: julian.hofbauer@htwk-leipzig.de, mathias.rudolph@htwk-leipzig.de)*
** *Technische Universität Chemnitz; Laboratory for Automatic Control and System Dynamics, 09107 Chemnitz, Germany (e-mail: stefan.streif@etit.tu-chemnitz.de)*

Abstract: For analysis of photovoltaic cells artificial light sources, so called solar simulators can be used. The light spectrum and light intensity of the considered LED solar simulators is time varying due to current induced heating of the semiconductor. The change influences the measurement accuracy for the characterisation of solar cells. With the current as a control variable, the light intensity can be stabilised. The drift in the light colour can only be compensated with spectrally adjacent LEDs. Based on known physical and phenomenological correlations concerning the behaviour of LEDs, model equations for the solar simulator were developed and simplified. The corresponding parameters were determined by experiments on a solar simulator. A LQG controller was designed for the stabilisation of the time-varying spectrum. The controller is tested in simulations for different light spectra. The improvements over the uncontrolled case are demonstrated.

Keywords: solar simulator, LQG control, LED, spectrum estimation, solar cells

1. INTRODUCTION

The adjustment or modification of the intensity or spectrum of light is relevant in many areas, such as the lighting of rooms or objects, ambient light at workplaces to improve working conditions, as well as for measurement tasks. With the use of LED technology as a light source, it is possible to control the light intensity as well as the light spectrum directly, without the additional use of colour filters. Especially for measurement tasks, the homogeneity and stability of the light spectrum is of particular importance.

As discussed in this work, for the characterisation of photovoltaic (PV) cells, even small changes in light intensity and spectrum (occurring during the measurement) affect the measurement accuracy. For the reproducible characterisation of photovoltaic cells, the measurement is performed at standard test conditions (STC). STC defines the temperature and the irradiance of the solar cell as well as the spectrum of the artificial light source.

The artificial sunlight can be generated by solar simulators. LED based solar simulators work with an array of different coloured current-controlled LEDs. The general requirements like spectral adaptations and temporal stability are defined in IEC 60904-9:2007. Thus, the artificial light spectrum should also correspond to the shape according to the spectrum at STC (application-specific adaptation of the spectrum is given in Scherff et al. (2017)). Further requirements are flexible spectra for different measurements as well as a freely configurable illumination time. For the analysis of solar cells, multiple measurements under different lighting conditions are performed in less than one second. It is therefore not possible to operate the LED solar simulator in a thermally stable state.

The LED light spectrum depends on the current and the junction temperature. With increasing time, the current induced heating of the junction increases until saturation. This results in a time varying light spectrum and impairs the measurement accuracy in the characterization of solar cells. Therefore a controller is required to regulate the temperature effect which keeps the light spectrum stable. The aforementioned requirements must be taken into account when selecting the controller. In particular, the shape of the spectrum, a constant irradiance over time, and a short settling time must be taken into consideration.

In the field of intensity and colour control of LEDs, the research papers of Tang et al. (2018), Lohaus et al. (2013) and Qu et al. (2007) should be mentioned among others. These mainly refer to the control of light in the perceptible area of the human eye (using colour matching function according to International Commission on Illumination - CIE). In addition to controllers which keep the light colour constant on the basis of the measured light intensity by the use of colour filters (usually for the colour components red, green, and blue), the forward voltage as equivalent to the junction temperature is often also measured for adjusting colour drifts (Lee et al. (2016); Schubert (2010); Xi et al. (2005b); Xi et al. (2005a); Muthu et al. (2002)). Depending on the application, the intensity of the individual light colours (measured using an intensity sensor and colour

filter) or the junction temperature is used as the control- or state variable, for controlling with a PI controller (Muthu et al. (2002); Qu et al. (2007)). When looking at the system as a multiple single input single output system, only the intensity of the individual LEDs is kept constant. The drift of the individual LED spectra, which affects the shape of the spectrum, is neglected.

In this paper the approach of a state controller (with temperature as state variable) is used to compensate for the drift of the light spectrum. Since the state variable cannot be measured directly for the given application, it must be determined from the measured total spectrum (resulting from the overlaid single LED spectra). Therefore an observer is used. Due to the noisy measurement signal (especially at low LED currents) the observer was designed as a Kalman-Filter. On the basis of the work required for the design of a Kalman-Filter, a state feedback controller can be designed as LQ controller with little additional effort. In the following, LQG as a combination of LQ control and Kalman-Filter is presented as an approach to compensate the drift of individual LEDs by adjacent LEDs and thus to control the shape of the spectrum.

The goal and main contribution of this work is the modelling of LED solar simulators and the design of an associated controller to stabilise the light spectrum as presented in Section 2 and Section 4. The focus is on the description of the dependencies (current, temperature dependency) of the artificial sunlight as a basis for the design of a multi-variable controller. The modelling of the system including the design of a state space model (non linear), the construction of a Kalman-Filter (state estimator) as well as the calculation of the LQ optimal gain are further addressed. As described in Section 3, the model parameters and the model verification were determined on the basis of measurements from an experiment. The controller was tested in simulations. The results are presented in Section 5.

2. MODELLING OF THE SOLAR SIMULATOR

2.1 Description of the LED Light Spectrum

The light spectrum of LED solar simulators changes with increasing (time-dependent) junction temperature primarily with respect to light intensity. Another temperature-based effect is the drift of the spectrum towards higher wavelength ranges (colour change). The amount of the changes depends on the LED semiconductor material. This means that the intensity of the changes varies depending on the wavelength range. It is therefore important to look at the composition of the LED based artificial light spectrum. The light spectrum of the solar simulator results from the sum of the n individual LED light spectra (Fig. 1) $I_{sum}(\lambda) = \sum_{n=1}^{m} I_n(\lambda)$.

Due to ageing of the semiconductor, the temperature behaviour of the LED also changes. To simplify matters, ageing is neglected in the following. To minimize the resulting deviation, for practical application, a cyclic calculation of the system parameters is necessary. The changes within these intervals are assumed to be very small, so that within these intervals a time invariant system can be assumed.

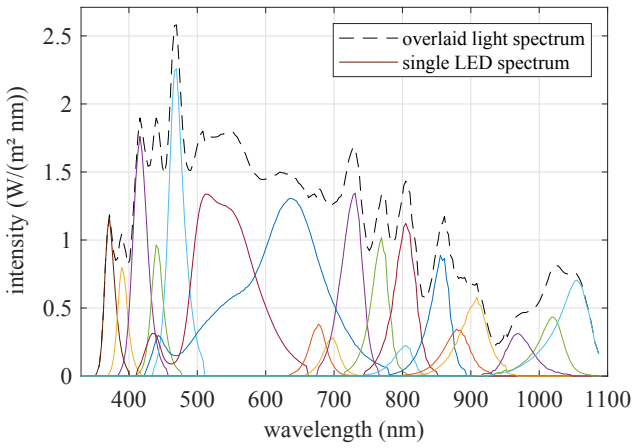

Fig. 1. Light spectrum of the solar simulator, single LED spectra

According to STC the light intensity is defined with 1000 W/m^2. The light spectrum should correspond to the sunlight under air mass AM1.5 defined in IEC 60904-3:2008.

The spectrum is defined as intensity (I) over the wavelength (λ). The behaviour of the n single LEDs is the basis for the resulting overall spectrum. The change in the overall spectrum results in the sum of the single changes. Individual differences must be taken into account. Under constant conditions (in terms of current and chiller temperature), a change in the light spectrum is due to the heating of the LED semiconductor. The corresponding value is the junction temperature of the n single LEDs $\vartheta_{J,n} = f(i, t, \vartheta_{chiller})$. The temperature induced change of the spectrum is shown in Fig. 2.

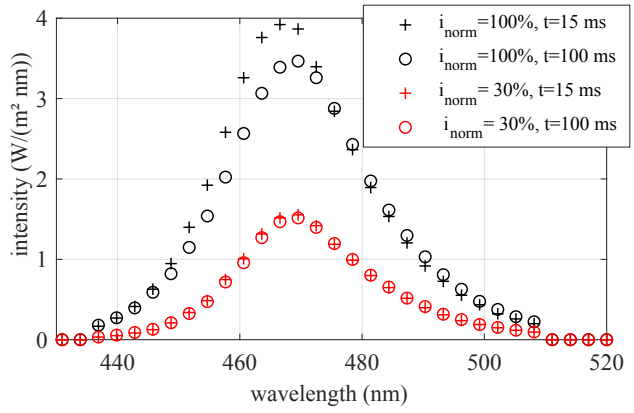

Fig. 2. LED spectrum as a function of current and time

In the following, the modelling of the light spectrum of a single LED is discussed. For the sake of clarity, the index n is omitted. Suitable parameters are required to quantify the behaviour of LED spectra. This is where the parameters of distribution functions come in, since the amplitude (A) can be used to describe the intensity behaviour, the center (c) to describe the drift of the spectrum, and the skewness (S) as well as the width (W) to describe the shape of the spectrum. Different distribution functions for the description of LED light spectra were

investigated. In Reifegerste and Lienig (2008) the approximation of the LED light spectrum via Logistic Power Peak function (LPP) fits best. The LPP describes the LED spectrum over the mentioned parameter A, c, S, and W as a function of wavelength (1). The parameters depend on current i, temperature ϑ_J, and the constants p_{km} ($k \in \{a, c, s, w\}, m \in \{0, T, i\}$) (2) - (5).

$$I(\lambda) = \frac{A}{S} \cdot (1 + \exp((\lambda - c + W \cdot \ln(S))/W)^{-(S-1)/S} \cdot \exp((\lambda - c + W \cdot \ln(S))/W) \cdot (S+1)^{(S+1)/S} \quad (1)$$

$$A(\vartheta_J, i) = p_{a0} \cdot \vartheta_J^{p_{aT}} \cdot i^{p_{ai}} \quad (2)$$

$$c(\vartheta_J, i) = p_{c0} + p_{cT} \cdot \vartheta_J + p_{ci} \cdot \log(i) \quad (3)$$

$$S(\vartheta_J, i) = p_{s0} + p_{sT} \cdot \vartheta_J + p_{si} \cdot \log(i) \quad (4)$$

$$W(\vartheta_J, i) = p_{w0} + p_{wT} \cdot \vartheta_J + p_{wi} \cdot i \quad (5)$$

With respect to the LPP distribution function, there is primarily a change in the parameters center c (peak wavelength) and amplitude A (the change in the shape with respect to parameters S and W is minimal). Depending on the semiconductor material used, the behaviours differ. Even with identical materials, manufacturer- and production-related variations in the temporal behaviour occur. Generally the change in amplitude is always greater than the drift of the spectrum.

In addition to the junction temperature, the current also affects the colour of the LED. The change in colour can be seen in (3) by the shift of the center c. Depending on the semiconductor material, the shift can be either towards shorter or longer wavelengths. On the example of two LED channels (channels 2 and 10) installed in the solar simulator Fig. 3 shows the dependence of the material. A LED channel is the combination of several LEDs of the same type. The peak wavelength, i. e. the position of the light spectrum, depends both directly and indirectly (via the junction temperature) on the current. For the controller design the consideration of the LEDs as single components (resp. as multiple single input single output system) is not sufficient to keep the shape of the spectrum constant.

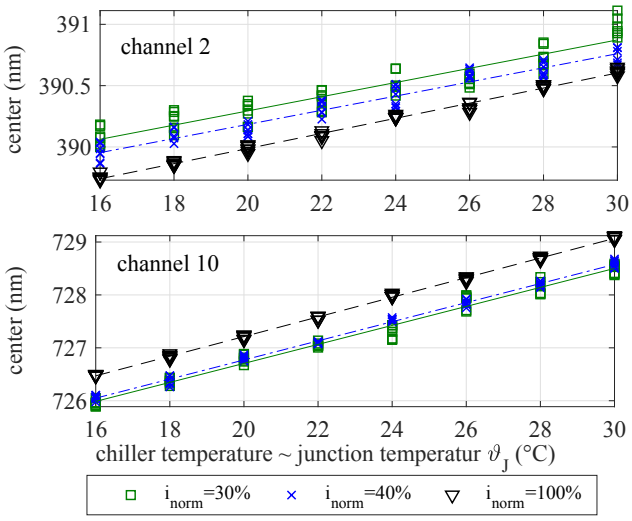

Fig. 3. Temperature response of peak wavelength, measurement data with linear approximation

Due to the shift of the peak wavelength and the defined (limited) number of LEDs in the solar simulator, the initial light spectrum (target spectrum) cannot be reproduced with absolute accuracy. The primary problem consists in combining the spectra of the single LEDs to a superimposed light spectrum via the current as control variable, so that the resulting light spectrum corresponds to the target spectrum as close as possible. Furthermore, the irradiance (intensity over all wavelength $\int_{\lambda_1}^{\lambda_k} I(\lambda)$) must be kept constant.

2.2 Time Response of the Junction Temperature

By default, like in Gu and Narendran (2004), Narendran et al. (2004), Thorseth (2011) and Reifegerste and Lienig (2008) among others, the LED junction temperature ϑ_J can be described by a thermal resistor R_{th}, power dissipation (thermal power P_{th}), and ambient temperature ϑ_{amb} (6).

$$\vartheta_J = P_{th} \cdot R_{th} + \vartheta_{amb} \quad (6)$$

With existing storage mass (or for short observation times) the approach described in (6) has to be extended by the storage behaviour (capacity) (transient heat conduction or RC network). The result is a thermal equivalent circuit diagram consisting of RC elements connected in series, a so called Foster network.

Based on Eleffendi and Johnson (2014) (7), (8) show the thermal impedance (frequency- and time domain) of a Foster network as well as the corresponding DGL (9) with r RC elements:

$$Z_{th}(s) = \sum_{i=1}^{r} \frac{p_{Z1i}}{s + p_{Z2i}} \quad (7)$$

$$Z_{th}(t) = \sum_{i=1}^{r} \frac{p_{Z1i}}{p_{Z2i}} (1 - e^{-t \cdot p_{Z2i}}) \quad (8)$$

with $p_{Z1i} = 1/C_i$, $p_{Z2i} = 1/(R_i \cdot C_i)$

$$d\Delta\vartheta/dt = A \cdot \Delta\vartheta + B \cdot P_{th} \quad (9)$$

$$\text{with } A = \begin{pmatrix} p_{Z21} & 0 & \cdots & 0 \\ 0 & p_{Z22} & \cdots & 0 \\ \vdots & \vdots & \ddots & \vdots \\ 0 & 0 & \cdots & p_{Z2r} \end{pmatrix}, B = \begin{pmatrix} p_{Z11} \\ p_{Z12} \\ \vdots \\ p_{Z1r} \end{pmatrix}$$

The thermal power (P_{th}) results from the difference between electrical (P_{el}) and optical power (P_{opt}) (10).

$$P_{th} = P_{el}(i, \vartheta_J) - P_{opt}(i, \vartheta_J) \quad (10)$$

The dependence of the light output P_{opt} on the current, for constant temperatures, can be described empirically according to (Thorseth, 2011, p. 23) by a second order polynomial. Under the given condition of a zero crossing (11) results.

$$P_{opt}(\vartheta_J = const) = p_{opt1} \cdot i + p_{opt2} \cdot i^2 \quad (11)$$

Taking into account the influence of temperature, based on (Schubert, 2010, pp. 98-99) the phenomenological equation (12) for temperatures close to room temperature results.

$$P_{opt} = P_{opt}|_{\vartheta_{ref}} \cdot \exp\left(\frac{-\vartheta_J - \vartheta_{ref}}{p_{opt3}}\right) \tag{12}$$

The parameter p_{opt3} is a constant depending on the semiconductor material of the LED, ϑ_{ref} is the reference temperature.

P_{el} is given with $P_{el} = i \cdot u(i, \vartheta_J)$ and can be determined with the approximate equation for $u(i, \vartheta_J)$ (13),

$$u(i, \vartheta_J) = (i \cdot p_{el1} + p_{el2})|_{\vartheta_0} + i \cdot p_{el3} \cdot \Delta\vartheta \tag{13}$$

and results in (14):

$$\begin{aligned} P_{th} = {} & i \cdot (i \cdot p_{el1} + p_{el2})|_{\vartheta_0} + i \cdot p_{el3} \cdot \Delta\vartheta \\ & -(p_{opt1} \cdot i + p_{opt2} \cdot i^2)|_{\vartheta_0} \cdot \exp\left(-\frac{\Delta\vartheta}{p_{opt3}}\right) \end{aligned} \tag{14}$$

with $p_{el_i}, p_{opt_i} = const.$

As shown in (1) - (5), the spectrum $I(\lambda)$ depends on the current i, and the junction temperature ϑ_J. The junction temperature is not directly measurable during operation and has to be determined experientially by means of auxiliary variables such as peak wavelength or forward voltage. Since the measured variable forward voltage is not given for the investigated application, the peak wavelength was used to determine the junction temperature. With the exception of LEDs with luminous layer, the peak wavelength can be determined from the measurement data. For LEDs with luminous layer the peak wavelength of the energising LED was determined. By substituting the junction temperature with the peak wavelength (center c), an easily identifiable state variable can be obtained for individual LEDs.

The solar simulator investigated is a system with 20 measurable LED channels. The measured or controlled variable y is the spectrum which consists of the intensity related to 256 wavelengths $I(\lambda_1 ... \lambda_{256})$ in the measuring range of 330 nm to 1087 nm ($y \in \mathbb{R}^{256}$). The actuating variables u are the currents i flowing through the 20 LEDs ($u \in \mathbb{R}^{20}$). The disturbance z is the thermal power which affects the 20 LEDs and the respective junction temperature ($z \in \mathbb{R}^{20}$). The state variable x is the normalised peak wavelength c_{norm} and proportional to the junction temperature ($x \in \mathbb{R}^{20}$), see also Fig. 7.

3. MODEL PARAMETER ESTIMATION USING EXPERIMENTAL DATA

In the first step the peak wavelength (substitution of junction temperature as state variable) was calculated from the measurement data for each time step (from $10 - 100$ ms) and for each set current. The approximate proportionality between peak wavelength and junction temperature given in Xi et al. (2005a); Chhajed et al. (2005); Reifegerste and Lienig (2008) was confirmed by own measurements for temperatures from 16 $°C$ to 30 $°C$ (Fig. 3). It was assumed that for very short exposure times, the measurable chiller temperature corresponds to the junction temperature. The measurement was therefore carried out for short light pulses with a duration of 10 ms (smallest value adjustable on the solar simulator).

The modelling of a single LED is based on (2), (3), and (7) - (14) simplified for a system of order one (one RC element) and a constant chiller temperature ($\vartheta_{chiller} = const$). The resulting state equation as a function of peak wavelength and current is given in (15).

$$\begin{aligned} \frac{dc_{norm,n}}{dt} = {} & p_{s1,n} \cdot c_{norm,n}(t) + p_{s2,n} + \\ & p_{s3,n} \cdot \log(i_n(t)) + i_n \cdot [i_n(t) \cdot (p_{s4,n} + \\ & p_{s5,n} \cdot \log(i_n(t))) + p_{s6,n} \cdot \log(i_n(t)) + \\ & p_{s7,n} \cdot i_n(t) \cdot c_{norm,n}(t) + p_{s8,n}] \end{aligned} \tag{15}$$

To simplify the problem of the high non-linearity of (1), the LPP function is not used to describe the light spectrum of an LED. Instead of using equation (1), the light output of each measurement point λ_m is described with P_{opt} by (12) with $m \in \{1, ..., 256\}$. The output equation is given in (16).

$$\begin{aligned} I_{\lambda_m} = \sum_{n=1}^{20} & i_n(t) \cdot (p_{o1,n}^{\lambda_m} + p_{o2,n}^{\lambda_m} \cdot i_n(t)) \cdot \\ & \exp(p_{o3,n}^{\lambda_m} + p_{o4,n}^{\lambda_m} \cdot \log(i_n(t)) + \\ & c_n(t) \cdot p_{o5,n}^{\lambda_m}) \end{aligned} \tag{16}$$

For the solar simulator with 20 different coloured LEDs $\dot{c}_{norm}$ is a vector with 20 elements ($\dot{c}_{norm,n}$ with $n \in \{1, ..., 20\}$). The elements $\dot{c}_{norm,n}$ can be calculated according to (15).

The parameters $p_{si,n}$ are calculated in MATLAB using a nonlinear least squares fitting procedure (`fitoptions('Method','NonlinearLeastSquares')`). With known parameters and known boundary conditions it is possible to simplify equation (15). The result is the simplified equation given in (17), for normalised currents greater than 10 %.

$$\begin{aligned} \frac{dc_{norm,n}}{dt} = {} & i_n(t) \cdot (p_{z1,n} + p_{z2,n} \cdot i_n(t)) + \\ & p_{z3,n} \cdot \log(i_n(t)) - \\ & p_{z4,n} \cdot c_{norm,n}(t) + p_{z5,n} \end{aligned} \tag{17}$$

For currents close to zero (15) or (17), are not applicable. For the defined observation range of the normalized currents, the logarithm can be approximated by a polynomial. The model equations can therefore also be used for currents close to zero. The output equation can also be simplified, this results in (18).

$$\begin{aligned} I_{\lambda_m} = \sum_{n=1}^{20} & i_n(t) \cdot (p_{a1,n}^{\lambda_m} + p_{a2,n}^{\lambda_m} \cdot i_n(t) + \\ & p_{a3,n}^{\lambda_m} \cdot \exp(-c_{norm,n}(t) \cdot p_{a4,n}^{\lambda_m})) \end{aligned} \tag{18}$$

Comparing equation (15) and equation (17) regarding the quality of the fit (see Fig. 4), no essential deterioration can be seen due to the simplification. The error difference between the individual channels is significantly greater than the increase in the error resulting from the simplification. The behaviour also applies to the output equation, where (16) is compared with (18).

To calculate the parameters $p_{z1,n}, ..., p_{z5,n}$ and $p_{a1,n}, ..., p_{a4,n}$, the spectra of the individual n LED channels were repeatedly measured for currents of $10 - 100$ % (normalised to the maximum value) on the solar simulator. Starting at 10 ms, the light spectrum was measured every 10 ms up to 100 ms. The parameters $p_{z1,n}, ..., p_{z5,n}$ were determined through $c_{norm,n}(t, i)$ using the solution

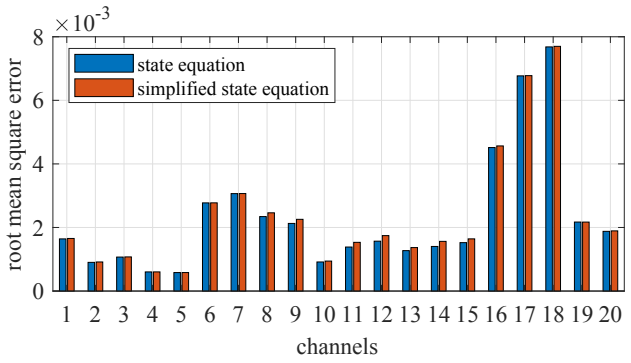

Fig. 4. Comparison of goodness of fit with respect to state equation and simplified state equation

equation of (17). This relationship can be seen in Fig. 5. The parameters $p_{a1,n}, ..., p_{a4,n}$ are determined analogue to $p_{z1,n}, ..., p_{z5,n}$ fitting (18) against measurement data.

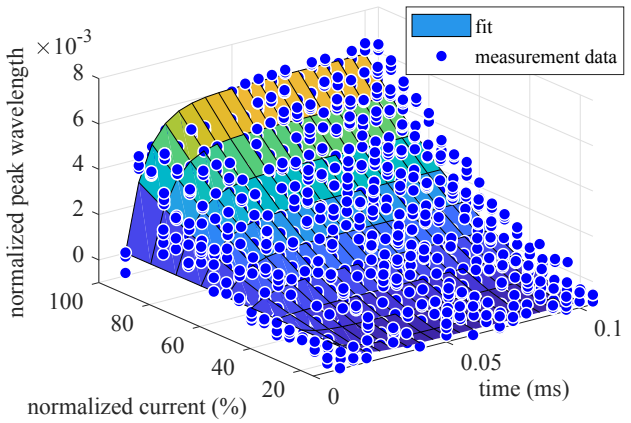

Fig. 5. Determination of the parameters $p_{z1,n}, ..., p_{z5,n}$ for channel 5

As shown in Fig. 6 and Tab. 1 the comparison of simulation and measurement data (uncontrolled) shows a good model quality over time. Also with regard to the dependence on the current (50% of the current intensity related to the standard spectrum - AM1.5/2), the simulation corresponds to the measured behaviour. The deviation (Root Mean Square Error RMSE) normalised to the maximum value of the intensity for the considered scenarios is between 2.55 % for the AM1.5 spectrum after a time of 15 ms and 1.50 % for the same spectrum after 100 ms.

Table 1. Model quality

scenario	RMSE norm
$AM1.5/2, t = 15\ ms$	1.75 %
$AM1.5/2, t = 100\ ms$	1.76 %
$AM1.5, t = 15\ ms$	2.55 %
$AM1.5, t = 100\ ms$	1.50 %

4. CONTROLLER FOR LIGHT SPECTRUM STABILISATION

The overlaid light spectrum of the solar simulator consist of a defined number of LEDs. Due to the white noise of the spectrometer data and the overlying LED spectra no clear determination of the peak wavelength c is possible. A state

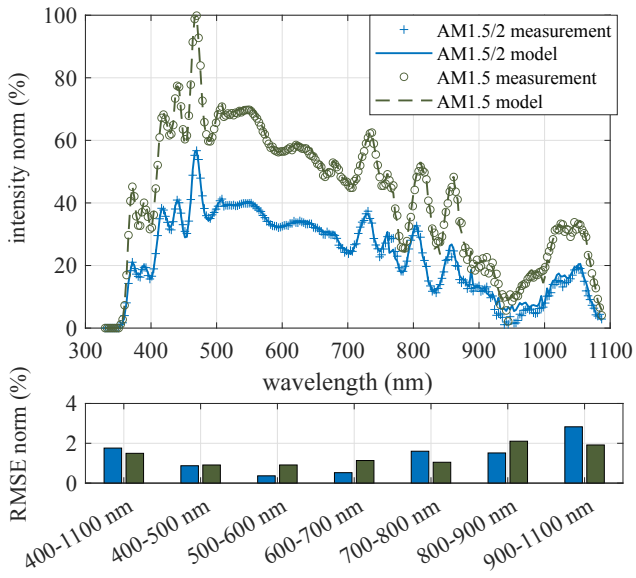

Fig. 6. Comparison model, measured values at $t = 100\ ms$

estimator (Kalman-Filter) can be used to determine the state values of the single LEDs for known currents. Based on this, the change in the spectrum depending on ϑ_J or c_{norm} can be controlled by a state feedback controller. In the following the calculation of estimator and controller as Linear-Quadratic-Gaussian (LQG) control is described. The basic principle can be seen in Fig. 7. With the normalized peak wavelength c_{norm} as state variable x, the spectrum $I(\lambda)$ as output variable y, the normalized current i_{norm} as control variable u (initial u_0, controller output $u_{controller}$), the process noise w, and the measurement noise ν. Furthermore, $\hat{x}$ and $\hat{y}$ are the estimated values for the state and output variable.

A linear model is required to calculate the feedback matrix of the Kalman-Filter $K_{estimator}$ as well as the feedback gain of the controller $K_{controller}$. The conversion of the non-linear behaviour into a linear model is done using the approach of linearisation by means of inverse characteristic (state equitation (17)) and linearisation in the operating point (output equation (18)). The operating point for the output equation was chosen to minimize the deviations of the linear model from the nonlinear model in the range $10 - 100$ % of the normalized LED current and the normalized peak wavelength for the time period $t = 0 ... 100\ ms$. This results in the standard form: $\dot{x} = A \cdot x + B \cdot u + w$; $y = C \cdot x + D \cdot u + \nu$ were A and B are diagonal matrices with $A \in \mathbb{R}^{20 \times 20}$ and $B \in \mathbb{R}^{20 \times 20}$. C and D are matrices in the form $C \in \mathbb{R}^{256 \times 20}$ and $D \in \mathbb{R}^{256 \times 20}$. The described system was tested for controllability and observability. Both are given.

For the design of the Kalman-Filter, the optimal feedback matrix ($K_{estimator}$) results from the general relationship $K_{estimator} = (P \cdot C^T + N_{Kf})R_{Kf}^{-1}$ (for simplification with $N_{Kf} = 0$) where P is the solution of the algebraic Riccati equation ($A \cdot P + P \cdot A^T - P \cdot C^T \cdot R_{Kf}^{-1} \cdot C \cdot P + Q_{Kf} = 0$). The matrices Q_{Kf} and R_{Kf} were determined from the disturbances with $Q_{Kf} = E\{ww^T\}$ and $R_{Kf} = E\{\nu\nu^T\}$, where w and ν are white Gaussian noise processes (Lunze, 1997, pp. 301-303).

To determine R_{Kf}, the noise in the measurement signal was calculated by the variance σ_ν^2 from the repetition of measurements. Therefore R_{Kf} was calculated via $R_{Kf} = I_n \cdot \sigma_\nu^2$ were I_n is a $n \times n$ identity matrix with $n = 256$. Q_{Kf} is calculated from the process noise w witch results from the variance σ_w^2 of the state variable determined by repeated measurements. Q_{Kf} is determined analogue to R_{Kf} with $Q_{Kf} = I_m \cdot \sigma_w^2$ were I_m is a $m \times m$ identity matrix with $m = 20$.

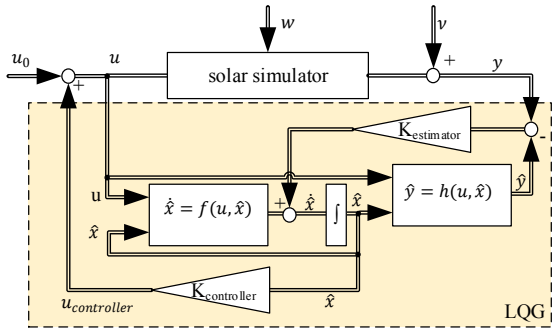

Fig. 7. Scheme LQG for the control of light spectra

The aim for the controller design is to keep the spectrum stable over time. The deviation from the initial output variable must therefore be minimised. The minimisation of the control energy should be considered as a secondary criterion for the control design. This results since the thermal energy increases with increasing input power and the drift of the spectrum is amplified (10), (14). Using the quadratic functional, this condition leads to the cost functions (19) (Lunze, 1997, pp. 261-264).

$$J(y_0, u) = \int_0^\infty (y(t)^T \cdot Q \cdot y(t) + u(t)^T \cdot R \cdot u(t))dt \quad (19)$$

The general form, with regard to the state variable is given in (20).

$$J(x_0, u) = \int_0^\infty (x(t)^T \cdot Q \cdot x(t) + u(t)^T \cdot R \cdot u(t) + 2 \cdot x(t)^T \cdot N \cdot u(t))dt \quad (20)$$

The choice of the weighting matrices Q, R, and N is decisive for the behaviour of the controller. Since the matrices influence each other, R was defined as an identity matrix and N was set to zero for simplification. The calculation of Q was performed according to the following scheme.

1. quantifying overlaps of LED spectra
   → relation Matrix (Q_{rel}) was created
2. quantifying share of LEDs in the total spectrum
   → share vector (q_{share}) was created
3. quantifying deviation between $t = 0\ ms$ and $t = 100\ ms$ for all channels
   → deviation vector (q_{dev}) was created
4. heuristic optimisation
   → weighting vector (q_w) was created
5. Hadamard product of the relation matrix with the share vector the deviation vector and the weighting vector (21)

$$\bar{Q} = Q_{rel} \circ q_{share} \circ q_{dev} \circ q_w \quad (21)$$

To calculate the gain matrix, care must be taken to ensure that the conditions, namely symmetry and positive definiteness, are satisfied for the weighting matrices Q, R, and N. The weighting matrix Q result as follows: $Q = \bar{Q}^T \cdot \bar{Q}$. It must be further ensured that the controller is optimal for all initial conditions x_0. This means that all eigenprocesses must be observable by the cost function. For this purpose the pair $(A, \bar{Q})$ must be observable. This was verified and confirmed.

5. SIMULATION RESULTS

The suitability of the developed LQG controller for different spectra was tested in simulation. The matrix Q was optimised with respect to the AM1.5 (standard spectrum). The quality criteria used are the maximum deviation of the total intensity, the deviation according to the ranges defined in IEC 60904-9:2007 and the shape of the spectrum in each case related to the initial value at time $t = 0$. A further criterion is the Key Performance Indicator (KPI). For the characterisation of PV, this refers to the short-circuit current i_{sc} of the solar cell (DUT). The KPI is calculated as follows: $\text{KPI} = (i_{sc,max} - i_{sc,min})/(i_{sc,max} + i_{sc,min})$. The short-circuit current is well suited as a quality criterion, it is influenced by the irradiance and the corresponding wavelengths. Since the short-circuit current also changes depending on the solar cell measured (e. g. different sensitivity with regard to individual wavelength ranges), this is not suitable as the only evaluation or optimisation criterion.

As shown in Fig. 8, the controller compensates the deviations from the target spectrum, whereby it is not possible to reach the target spectrum. This is also due to the hardware technical conditions. So it is not possible in all areas to compensate the drift by adjacent LEDs. The temporal course is given in Fig. 9 for the quality characteristic short-circuit current (of the DUT).

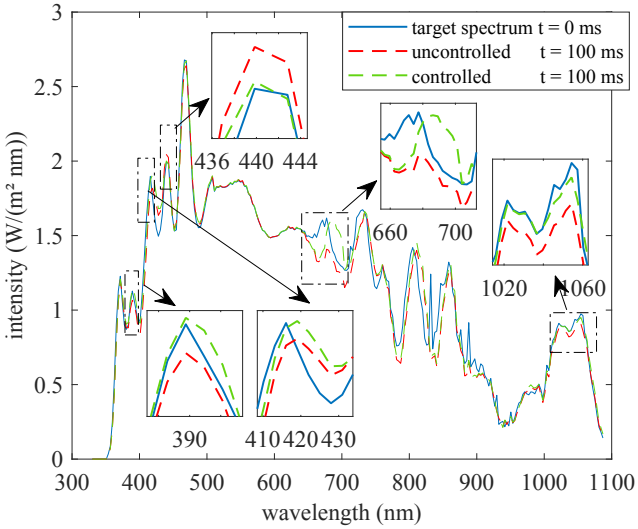

Fig. 8. Comparison of the uncontrolled and controlled AM1.5 spectrum

Tab. 2 shows in the top part, the deviation of the irradiance ΔI of the light spectrum related to the time $t = 0\ ms$ and $t = 100\ ms$ for defined wavelengths according to

IEC 60904-9:2007. The irradiation results from the integration of the spectrum over the wavelength. The parameters were calculated for four scenarios the controlled ΔI_c and uncontrolled ΔI_u case, for the AM1.5 spectrum and for comparison the half AM1.5 spectrum (AM1.5/2). The second part of Tab. 2 shows the temporal deviation of the short circuit current Δi_{sc} and the KPI value for the four scenarios.

Table 2. Comparison of the deviation from the target state in (%):

Spectrum	**AM1.5/2**		**AM1.5**	
	ΔI_u	ΔI_c	ΔI_u	ΔI_c
400 500 *nm*	-0.16	-1.78	0.02	-1.37
500 600 *nm*	-0.25	-0.27	-0.24	-0.25
600 700 *nm*	2.51	-2.65	4.29	0.08
700 800 *nm*	2.81	0.59	4.38	1.63
800 900 *nm*	1.75	-1.37	5.55	2.75
900 1087 *nm*	1.93	-1.86	3.29	-0.08
400 1087 *nm*	1.24	-1.21	2.46	-0.23
	$\Delta i_{sc,u}$	$\Delta i_{sc,c}$	$\Delta i_{sc,u}$	$\Delta i_{sc,c}$
330 1087 *nm*	1.49	-1.32	2.97	0.55
	KPI$_u$	**KPI**$_c$	**KPI**$_u$	**KPI**$_c$
330 1087 *nm*	0.75	0.73	1.51	0.49

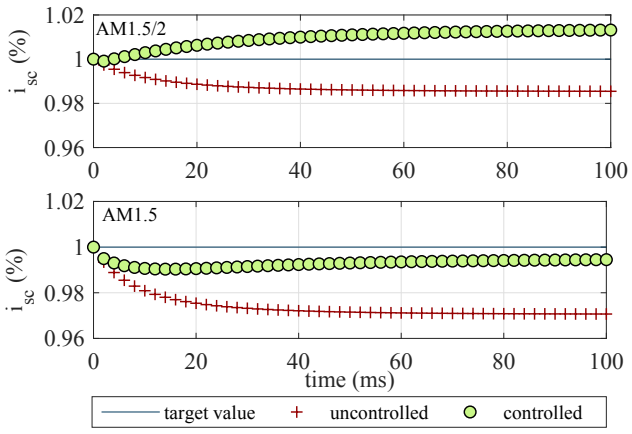

Fig. 9. Comparison ISC over time uncontrolled, controlled with Q optimised for the AM1.5 spectrum

For the AM1.5 spectrum, as can be seen in Fig. 9 and Tab. 2, a significant improvement to the uncontrolled case can be achieved. Outside the working point, as can be seen in the example of the half AM1.5 spectrum, the selected weighting matrix Q achieves a minimal improvement with respect to the criteria irradiance, short-circuit current, and KPI. For the AM1.5 as well as for the half AM1.5 spectrum the controller shows a weaker behaviour with respect to irradiance in the range $400 - 500\ nm$, than in the uncontrolled case. As can be seen in Fig. 8, also in the range $400 - 500\ nm$ the controlled spectrum shows a good adaptation to the shape of the initial spectrum. It is shown that the consideration of the irradiance can lead to misinterpretations, if there are positive as well as negative deviations within the considered wavelength range.

By changing the weighting matrix Q, the behaviour can be adapted so that the controller can also be used outside the operating point. This has an effect on the control quality in the operating point. This is shown by the example of the short-circuit current of the DUT in Fig. 10.

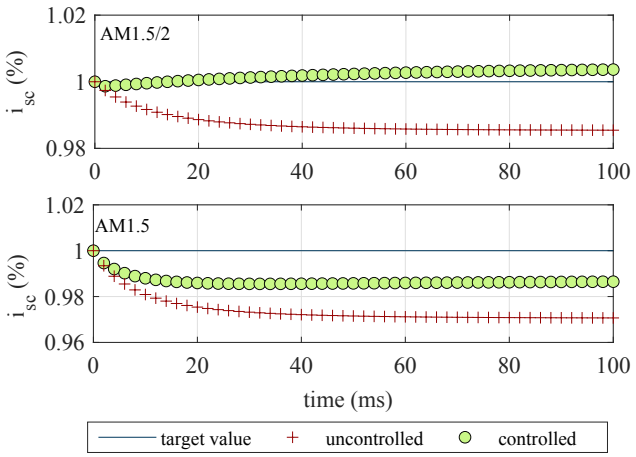

Fig. 10. Comparison ISC over time uncontrolled, controlled, with Q adapted for multiple spectra

6. SUMMARY AND CONCLUSION

Starting with the modelling of a single LED, the behaviour of solar simulators was described using a state space model. This provides the basis for the calculation of a Kalman-Filter and a LQ controller. As shown in simulation studies, the reduction and drift of light intensity and light spectrum can be compensated by means of LQG, whereby the target variable has not yet been reached and the system shows a permanent control deviation. Since it is not possible with the current setup to keep the spectrum in its initial value with the existing number of LEDs, a new distribution of the individual LEDs must be found which corresponds as closely as possible to the target spectrum. By selecting Q it is possible to set the spectrum with regard to the selected quality criterion such as short-circuit current or shape for a defined application.

In addition, the designed controller will be tested on a test rig as well as on the target system solar simulator. Furthermore, an adaptation of the LQG controller is planned so the light spectrum can be kept stable outside the operating point.

ACKNOWLEDGEMENTS

The work presented was carried out within the FHprofUnt project "FuzzySun" (funding code FKZ 03FH024PX5). The project was funded by the Federal Ministry of Education and Research (BMBF), for which we would like to thank. We would also like to thank our project partner, WAVELABS Solar Metrology Systems GmbH, for the application-specific provision of equipment and information.

REFERENCES

Chhajed, S., Xi, Y., Li, Y.L., Gessmann, T., and Schubert, E.F. (2005). Influence of junction temperature on chromaticity and color-rendering properties of trichromatic white-light sources based on light-emitting diodes. *Journal of Applied Physics*, 97(5).

Eleffendi, M.A. and Johnson, C.M. (2014). Thermal path integrity monitoring for IGBT power electronics modules. In *CIPS 2014, 8th International Conference on In-*

tegrated Power Electronics Systems. IEEE, Piscataway, NJ.

Gu, Y. and Narendran, N. (2004). A non-contact method for determining junction temperature of phosphor- converted white LEDs. In S.A. Stockman, H.W. Yao, and E.F. Schubert (eds.), *Light-emitting diodes*, Proceedings of SPIE. SPIE, Bellingham, Wash.

Lee, A.T.L., Chen, H., Tan, S.C., and Hui, S.Y. (2016). Precise dimming and color control of LED systems based on color mixing. *IEEE Transactions on Power Electronics*, 31(1), 65–80.

Lohaus, L., Leicht, E., Dietrich, S., Wunderlich, R., and Heinen, S. (2013). Advanced color control for multicolor LED illumination systems with parametric optimization. In *IECON 2013*, 3305–3310. IEEE, Piscataway, NJ.

Lunze, J. (1997). *Regelungstechnik 2: Mehrgrößensysteme, digitale Regelung*. Springer-Lehrbuch. Springer, Berlin, 1. edition.

Muthu, S., Schuurmans, F.J., and Pashley, M.D. (2002). Red, green, and blue LED based white light generation: Issues and control. In *Conference record of the 2002 IEEE Industry Applications Conference*, 327–333. IEEE, Piscataway, N.J.

Narendran, N., Gu, Y., and Hosseinzadeh, R. (2004). Estimating junction temperature of high-flux white LEDs. In S.A. Stockman, H.W. Yao, and E.F. Schubert (eds.), *Light-emitting diodes*, volume v. 5366 of *Proceedings of SPIE*. SPIE, Bellingham, Wash.

Qu, X., Wong, S.C., and Tse, C.K. (2007). Color control system for rgb LED light sources using junction temperature measurement. In *33rd annual conference of the IEEE Industrial Electronics Society, 2007*, 1363–1368. IEEE Service Center, Piscataway, NJ.

Reifegerste, F. and Lienig, J. (2008). Modelling of the temperature and current dependence of LED spectra. *Journal of Light & Visual Environment*, 32(3), 288–294.

Scherff, M.L.D., Nutter, J., Fuss-Kailuweit, P., Suthues, J., and Brammer, T. (2017). Spectral mismatch and solar simulator quality factor in advanced LED solar simulators. *Japanese Journal of Applied Physics*, 56(8S2).

Schubert, E.F. (2010). *Light-emitting diodes*. Cambridge Univ. Press, Cambridge, 2. edition.

Tang, S.J.W., Kalavally, V., Ng, K.Y., Tan, C.P., and Parkkinen, J. (2018). Real-time closed-loop color control of a multi-channel luminaire using sensors onboard a mobile device. *IEEE Access*, 6, 54751–54759.

Thorseth, A. (2011). *Characterization, Modeling, and Optimization of Light-Emitting Diode System*. Faculty of Science, University of Copenhagen.

Xi, Y., Xi, J.Q., Gessmann, T., Shah, J.M., Kim, J.K., Schubert, E.F., Fischer, A.J., Crawford, M.H., Bogart, K.H.A., and Allerman, A.A. (2005a). Junction and carrier temperature measurements in deep-ultraviolet light-emitting diodes using three different methods. *Applied Physics Letters*, 86(3), 031907.

Xi, Y., Gessmann, T., Xi, J., Kim, J.K., Shah, J.M., Schubert, E.F., Fischer, A.J., Crawford, M.H., Bogart, K.H.A., and Allerman, A.A. (2005b). Junction temperature in ultraviolet light-emitting diodes. *Japanese Journal of Applied Physics*, 44(10), 7260–7266.